

MicroRNA-148a Controls Epidermal and Hair ^{JID}Open Follicle Stem/Progenitor Cells by Modulating the Activities of ROCK1 and ELF5

Maximillian E. Pickup¹, Anhua Hu¹, Hetal J. Patel¹ and Mohammed I. Ahmed¹

Skin and hair development is regulated by complex programs of gene activation and silencing and microRNA-dependent modulation of gene expression to maintain normal skin and hair follicle development, homeostasis, and cycling. In this study, we show that miR-148a, through its gene targets, plays an important role in regulating skin homeostasis and hair follicle cycling. RNA and protein analysis of miR-148a and its gene targets were analyzed using a combination of *in vitro* and *in vivo* experiments. We show that the expression of miR-148a markedly increases during telogen (bulge and hair germ stem cell compartments). Administration of anti-sense miR-148a inhibitor into mouse skin during the telogen phases of the postnatal hair cycle results in accelerated anagen development and altered stem cell activity in the skin. We also show that miR-148a can regulate colony-forming abilities of hair follicle bulge stem cells as well as control keratinocyte proliferation/differentiation processes. RNA and protein analysis revealed that miR-148a may control these processes by regulating the expression of Rock1 and Elf5 *in vitro* and *in vivo*. These data provide an important foundation for further analyses of miR-148a as a crucial regulator of these genes target in the skin and hair follicles and its importance in maintaining stem/progenitor cell functions during normal tissue homeostasis and regeneration.

Journal of Investigative Dermatology (2022) ■, ■-■; doi:10.1016/j.jid.2022.06.028

INTRODUCTION

Skin development is a complex and dynamic process that results in the formation of a fully formed stratified epidermis with self-renewing capabilities, including several skin appendages, such as hair follicles (HFs) (Blanpain and Fuchs, 2009; Hsu et al., 2014). HF development and cycling processes are regulated by a well-balanced relationship between cell proliferation, differentiation, and apoptosis. These processes are controlled at several levels, including epigenetic, signaling/transcription factor-mediated, and microRNA mechanisms. MicroRNAs (miRNAs) (or miRs) are small noncoding RNAs involved in the post-transcriptional regulation of gene expression. miRNAs provide an additional level of regulation of important cellular processes such as growth, differentiation, and remodeling of the skin (Ahmed et al., 2014, 2011; Aunin et al., 2017; Mardaryev et al., 2010).

MiRNAs are ~22 nucleotides long and highly conserved, and their regulation is based on their interactions with target mRNAs by base-pairing between 5' end sequences of miRNAs and mRNAs sequences located in the 3' untranslated region. This results in either mRNA destabilization, inhibition

of translation initiation, or both, impacting important cellular pathways, such as cellular proliferation and differentiation. Thus, miRNAs principally contribute to the regulation of gene expression by fine tuning and buffering the activity of signaling pathways (Ambros, 2001; Lee et al., 1993; O'Brien et al., 2018; Pong and Gullerova, 2018). MiRNAs and their targets characterize remarkable regulatory networks, which have a crucial role in the regulation of gene expression programs in stem cells (SCs) and their progenies (Ambros, 2001; Inui et al., 2010; Zhang et al., 2011).

Principal studies have identified ~70 miRNAs and >200 miRNAs, which are dynamically expressed in mouse embryonic skin and during skin and HF cyclic regeneration, respectively (Andl et al., 2006; Mardaryev et al., 2010; Yi et al., 2006). In addition, epidermal-specific deletion of the miRNA processors *DICER*, *DORSHA*, or *DGCR8* results in severe abnormalities in skin and HF development and growth (Andl et al., 2006; Teta et al., 2012; Yi et al., 2009, 2006). These findings highlight the crucial role miRNAs have in the control of gene expression programs during skin and hair cycle-associated tissue remodeling.

Furthermore, individual miRNAs have been identified to be involved in controlling the expression of key regulators of cutaneous SCs and their lineage-committed progenies that control skin and HF development, homeostasis, and regeneration: miR-203 controls the proliferative potential of epithelial precursor cells (Lena et al., 2008; Yi et al., 2008), miR-125b serves as a rheostat that controls SC proliferation and differentiation (Zhang et al., 2011), and miR-205 is indispensable for SC survival (Wang et al., 2013a). Whereas miR-214 is a key regulator of SC functions during normal tissue homeostasis and regeneration (Ahmed et al., 2014), miR-31 controls hair cycle-associated tissue remodeling

¹School of Science and Technology, Nottingham Trent University, Nottingham, United Kingdom

Correspondence: Mohammed I. Ahmed, School of Science and Technology, Nottingham Trent University, Nottingham NG11 8NS, United Kingdom. E-mail: mohammed.ahmed@ntu.ac.uk

Abbreviations: HF, hair follicle; K, keratin; KC, keratinocyte; miRNA, microRNA; PMEK, primary mouse epidermal keratinocyte; SC, stem cell; WT, wild-type

Received 18 March 2022; revised 9 May 2022; accepted 16 June 2022; accepted manuscript published online XXX; corrected proof published online XXX

(Mardaryev et al., 2010). Recently, miR-218 was shown to regulate postnatal skin and HF development through the Wnt signaling pathway (Zhao et al., 2019). These findings highlight the importance of miRNAs in the control of gene expression programs during skin development and hair cycle-associated tissue remodeling.

Although substantial progress has been made in discovering the important regulators in the skin and HF development and homeostasis, understanding the molecular mechanisms involved in the establishment of signaling/transcription networks in keratinocytes (KCs) still requires additional efforts. In this study, we aimed to explore the role of miR-148a in regulating stem/progenitor cells during skin and HF development and regeneration. miR-148a has been identified as an oncosuppressor in various cancers (Takahashi et al., 2012; Wang et al., 2013b), including in the skin (Luo et al., 2015; Tian et al., 2015). However, its role in the control of skin and HF development and homeostasis remains unknown.

In this study, we identify miR-148a as a contributor to stem/progenitor cell activities in maintaining skin and HF development and homeostasis, at least in part, by regulating Rock1 and Elf5. We show that miR-148a shows distinct expression patterns in the epidermis and HF stem/progenitor cell compartments during hair cycle-associated tissue remodeling. Modulation of miR-148a activities can affect SC colony formation as well as KC proliferation and differentiation processes in vitro. Although in vivo, loss of miR-148a can lead to anagen progression and irregular expression patterns of SCs and differentiation during postnatal development.

RESULTS

MiRNA-148a is expressed in distinct stem/progenitor cell population in the skin and HFs

To understand the role of miR-148a in the control of skin and HF development/homeostasis and regeneration, miR-148a expression pattern was determined in C57Bl/6 wild-type (WT) mouse dorsal skin during postnatal and depilation-induced hair cycles. During spontaneous postnatal skin and HF development, we observed low miR-148a expression levels in the skin on postnatal day 12, with its expression increasing significantly during HF transition to the first regressing phase (catagen, postnatal days 16–17) and elevated further during subsequent resting phase (telogen, postnatal days 20–23) (Figure 1a). Similar fluctuations in miR-148a expression levels were observed in adult skin during depilation-induced hair cycle: miR-148a expression progressively decreased during HF transition from being its highest at the telogen stage (day 0) to significantly dropping in expression during anagen and catagen stages (day 3–19) (Figure 1b). Because CD34 is uniquely expressed in and is used to isolate mouse HF-bulge SCs (Blanpain et al., 2004; Trempus et al., 2003); therefore, we employed FACS sorting and identified that the expression of miR-148a was significantly higher in HF-bulge SCs populations (CD34⁺ cells vs. CD34⁻ cell populations) (Figure 1c).

We followed this analysis with in situ hybridization in postnatal and depilation-induced hair cycle (Figure 1d). Consistent with our reverse transcription quantitative

real-time PCR data, during the depilation-induced hair cycle, we observed high expression of miR-148a in telogen skin localized predominately in the epidermis (suprabasal layer) and in the telogen HFs (bulge and secondary hair germ regions). Although in subsequent stages, reduced expression was seen in early anagen (day 5), with a lack of expression seen in full anagen HFs (day 12) and catagen HFs (day 18) (Figure 1d). We subsequently performed FISH with simultaneous immunofluorescent staining, and we observed that miR-148a colocalizes with SC makers cytokeratin 15 (keratin [K] 15) and CD34 in telogen HFs (bulge and secondary hair germ regions). In the skin, miR-148a is predominantly expressed in the suprabasal layer of the epidermis compared with K15, which is expressed in the basal layer (Figure 1e).

Inhibition of miR-148a activity in the skin accelerates telogen–anagen development and alters SC activity

To explore the role of miR-148a in the control of hair cycle-associated tissue remodeling, a synthetic inhibitor that specifically binds and blocks miR-148a activity was administered to the dorsal skin of WT mice at different time points of spontaneous hair cycle. Owing to miR-148a expression being the highest during postnatal days 20–23 (Figure 1a), we administered anti-miR-148a daily into dorsal skin during the postnatal days 20, 21, and 22, and skin was harvested on postnatal day 23 (Figure 2a–g). The efficiency of inhibiting miR-148a activity was assessed by TaqMan RT-qPCR assay and showed a significant decrease in miR-148a expression in the skin treated with miR-148a inhibitors versus that in the controls (Supplementary Figure S1).

Inhibition of miR-148a activity during postnatal days 20–22 resulted in acceleration of telogen–anagen progression compared with that of the controls (Figure 2a–g). In mice treated with anti-miR-148a, significantly more HFs were found in anagen III stage, characterized by enlarged dermal papilla partially enclosed by KCs, whereas many HFs in the control skin reached only the anagen II phase of the hair cycle (Figure 2a–g). Acceleration of telogen–anagen development in skin treated with anti-miR-148a versus with controls was also associated with an increase in the skin thickness (Figure 2e), a well-established parameter of the hair cycle progression (Hansen et al., 1984; Mardaryev et al., 2010). To determine whether miR-148a has an impact on skin and HF stem/progenitor cell populations, we performed immunohistochemical staining. We observed an increased expression of K15⁺ SCs in the epidermis and in HFs of miR-148a-inhibited skins compared with that of the controls (Figure 2f). These changes in expression were confirmed by quantitative immunofluorescence analysis, which revealed increased expression of K15 in anti-miR-148a-treated versus in control skins (Figure 2g). These data suggest that an early or abnormal activation/expansion of SCs has occurred after inhibition. We next isolated mouse HF-bulge SCs from WT C57Bl/6 mice skin and compared colony formation capabilities in vitro. We observed a significant increase in the total number of colonies and the formation of larger holoclonal colonies (>50 μ m) after miR-148a loss compared with that of the

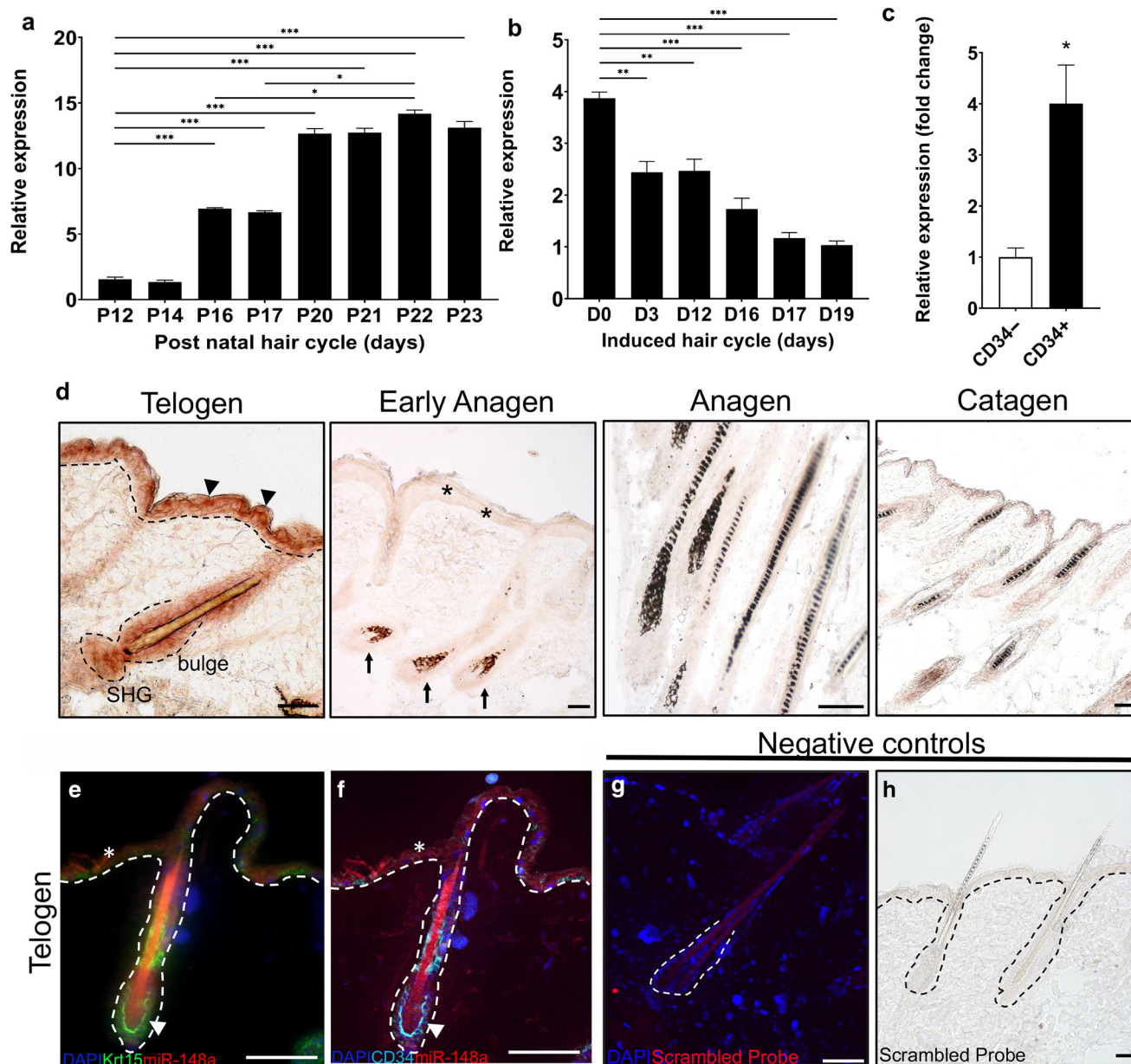


Figure 1. Spatiotemporal expression analysis of miRNA-148a during skin and HF development and regeneration. (a–c) TaqMan RT-qPCR analysis of miR-148a expression. (a) MiR-148a levels in the skin during the postnatal hair cycle days: anagen stage (P12), catagen (P16–P17), and telogen (P20–P23). miR-148a expression was elevated and reached its highest point during telogen stages (P20–23). $n = 3$ mice were used per stage. Data are presented as mean \pm SEM (error bars). (b) miR-148a in depilation-induced hair cycle: telogen (day 0), anagen (days 3 and 12), and catagen (days 17 and 19). miR-148a expression was elevated at the telogen stage (day 0) and significantly dropped in expression during all subsequent hair cycle stages. $n = 3$ mice were used per stage. Data are presented as mean \pm SEM values. Data are presented as mean \pm SEM. (c) FACS cell sorting: C57Bl/6 wild-type mice aged 7–9 weeks were used to isolate HF-bulge stem cells. miR-148a expression is elevated in CD34⁺ HF-bulge stem cells compared with that in CD34⁻ cells. $n = 3$ mice were used per experiment. Data are presented as mean \pm SEM values from three independent experiments. (d) miR-148a *in situ* hybridization. Depilation-induced hair cycle: miR-148a expression was detected in the stem cell compartments of telogen HFs (bulge and secondary hair germ). Furthermore, miR-148a expression in the epidermis was restricted to the differentiated, outermost suprabasal layer (arrowheads). Expression of miR-148a is dramatically reduced in early anagen skin (day 5, asterisks) and hair bulb (arrows) of HFs, and expression is absent from subsequent hair cycle stages (anagen and catagen). (e, f) miRNA-148a FISH with immunofluorescent staining of miR-148a (red) and stem cell markers cytokeratin 15 (K15, green) and CD34 (pseudo-colored cyanine) and DAPI (blue) in telogen stage of hair cycle. We observed the colocalization of miR-148a expression with both stem cell markers in the bulge (miR-148a⁺/K15⁺/CD34⁺) and secondary hair germ stem cell (miR-148a⁺/K15⁻/CD34⁻) compartments (arrowheads) of telogen HFs, whereas in the epidermis, K15 (basal layer) and miR-148a (suprabasal layer, asterisk) were predominantly mutually exclusive expressed. (g, h) The scrambled negative controls using (g) fluorescent and (h) chromogenic detections. Images are representative microphotographs of each stage and staining. The broken lines demarcate the epidermal–dermal border. * $P < 0.05$, ** $P < 0.01$, and *** $P < 0.001$ by Student's *t*-test. Bars = 50 μ m. P denotes postnatal day. HF, hair follicle; K15, keratin 15.

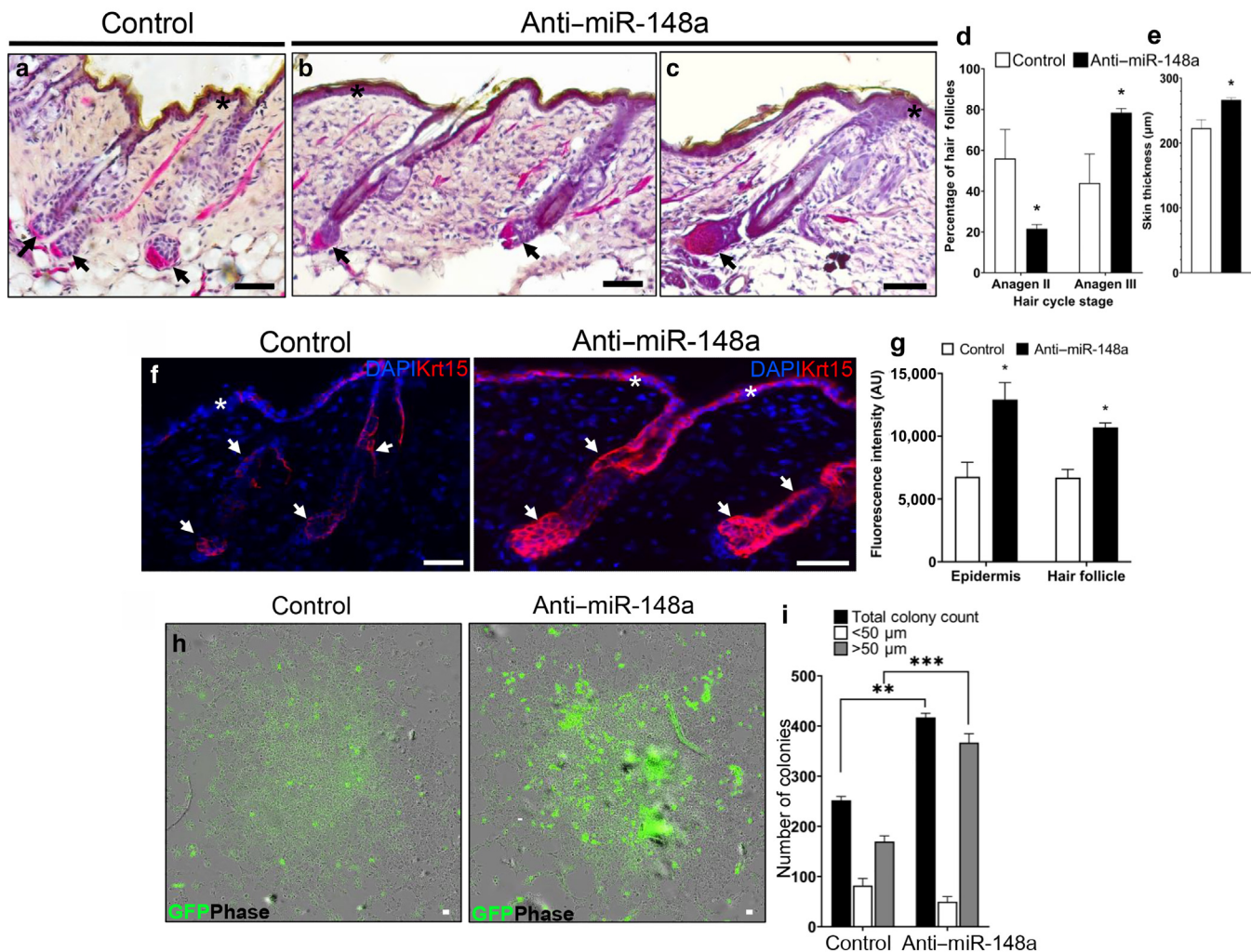


Figure 2. Inhibition of miRNA-148a accelerates telogen-anagen transition and alters stem cell activity. (a–f) Anti-miR-148a (inhibitor) or miRIDIAN-negative control were administered daily subcutaneously at postnatal skin days P20–P22. The skin was harvested on P23. In each experiment, ≥ 3 or 4 mice per time point were used for analyses in both anti-miR-148a and control groups. (a–c) Representative microphotographs of skin examples of (ai) control and (ai–iii) anti-miR-148a-treated skin on P23; sections were stained for the detection of endogenous alkaline phosphatase activity to visualize the morphology of dermal papilla as an important indicator of the defined stages in HF cycle. In control skins, the epidermis remained thin (panel a, asterisk) compared with anti-miR-148a-treated skins (panel b and c, asterisks). HFs of anti-miR-148a-treated skins observable had progressed to the anagen III stage, characterized by the presence of enlarged dermal papilla partially enclosed by keratinocytes (panels b and c, arrows), whereas most HFs in the control skin reached only anagen II phase in control-treated skins (panel a, arrows). (d) The percentage of HFs in defined stages of postnatal development was evaluated in cryostat sections of the skin of control or anti-miR-148a-treated mice by quantitative histomorphometry using established morphological criteria (Müller-Röver et al., 2001); there was a significant increase in the percentage of HFs in anagen III stage in anti-miR-148a-treated skins, compared with that of the controls, which were predominately in anagen II. Data are presented as mean \pm SEM values from 100 HFs counted per treatment. (e) Skin thickness after anti-miR-148a treatment is significantly increased, compared with that of the controls. Data are presented as mean \pm SEM values. (f) Cytokeratin 15 (K15) expression analysis by immunofluorescence. In anti-miR-148a-treated skin, increased expression of K15 is observed in the bulge region and developing hair bulb (panel f, arrows) compared with that of the controls (panel f, arrows). In the epidermis, K15 expression is also increased and continuous throughout the basal layer of anti-miR-148a treated skin (panel f, asterisks) compared with that of control epidermis where expression is lower and irregular (panel f, asterisk). Images are representative microphotographs of staining observed. (g) Quantitative immunofluorescence analysis: immunodetection of K15⁺ cells in the epidermis and HFs (red fluorescence) of control versus anti-miR-148a-treated skin samples normalized to DAPI⁺ cells. $n = 3$ mice per treatment. Data are presented as mean \pm SEM (error bars). (h) Colony-forming assay: inhibition of miR-148a expression using lentiviruses increases the capacity of HF-bulge stem cells to form colonies. Successful transduction of lentiviral particles was confirmed by the presence of GFP in cultured HF-bulge stem cells. (i) Quantification of the size and number of stem cell colonies formed after anti-miR-148a inhibition versus controls. An increase in the total number of colonies and larger colonies (>50 μ m in diameter) were observed in miR-148a-inhibited stem cells compared with that of the controls. Data are presented as mean \pm SEM values from five independent experiments. * $P < 0.05$, ** $P < 0.01$, and *** $P < 0.001$ by Student's *t*-test. Bars = 50 μ m. P denotes postnatal day. HF, hair follicle; K15, keratin 15.

controls (Figure 2h and i). Successful knockdown of miR-148a in HF-bulge SCs compared with that of the controls was confirmed by TaqMan RT-qPCR (data not shown).

MiRNA-148a overexpression induces complex changes in gene expression programs in KCs

To explore the molecular mechanisms of miR-148a in primary mouse epidermal KCs (PMEKs), RNA-sequencing

analysis was performed after overexpression of miR-148a (pro-miR-148a) versus that of the controls (Figure 3a). Functional ontology programs (<https://usegalaxy.org/>) were used to categorize differentially expressed genes into a set of 12 distinct functional categories. These were then ranked into groups with the most significantly changed genes, which included differentiation and cell cycle category groups (Figure 3b). To identify putative miR-148a gene targets, we performed bioinformatics analysis using well-established miRNA target prediction tools (Ahmed et al., 2019; Mardaryev et al., 2010). By overlapping predicted miR-148a targets from three different databases, we identified 408 potential genes whose expression may be regulated by miR-148a. To further refine this list, we overlapped these 408 genes with our RNA-sequencing data, genes that were significantly downregulated (859 genes) in pro-miR-148a versus in controls (Figure 3c). We selected genes for RT-qPCR validation with predicted binding sites as well as genes known to have important regulatory roles in epithelial development (a total of 43 gene targets). RT-qPCR analysis revealed that only *Rock1* and *Elf5* were significantly upregulated and/or downregulated of the genes analyzed after gain-or-loss of miR-148a, respectively (Figure 3d and e and Supplementary Figure S2).

Our analysis then focused on the effects of miR-148a on Rock1 and Elf5 protein levels: we observed that protein levels increased and/or decreased after gain-or-loss of miR-148a, respectively (Figure 3f). We next confirmed the direct regulation of Rock1 and Elf5 by miR-148a using a luciferase reporter assay. Cotransfection of HaCaT cells with pro-miR-148a mimic (overexpression) and either *Rock1* or *Elf5* 3' untranslated region reporter construct caused a significant reduction in luciferase activity, respectively, compared with that of their corresponding controls, whereas these effects were not detected when miR-148a-binding sites were mutated (Figure 3g).

In addition, we performed FISH for miR-148a with simultaneous immunofluorescence detection of Rock1 and Elf5 in WT telogen skin. In the epidermis, miR-148a, Rock1, and Elf5 were expressed mutually exclusively, where miR-148a is primarily expressed in the suprabasal layer, whereas Rock1 and Elf5 expression are predominately observed in the basal layer. We also observed that ROCK1 and ELF5 were coexpressed with miR-148a within SC compartments of HFs (bulge and secondary hair germ) (Figure 3h and i and Supplementary Figure S3).

Modulation of miR-148a activities alters the expression of key regulators during KC proliferation and differentiation

Our bioinformatic analysis revealed differentially expressed genes that belong to the cell cycle and differentiation categories (Figure 3b), which were further investigated.

Using RT-qPCR, we confirmed that the transcript levels of *Cdk16*, *Cdk1*, *Ccnb2*, *Ccne1*, *Ccnd1*, *Ccnd2*, and *Cksβ1* were significantly increased and/or decreased after modulation of miR-148a activity (Figure 4a and b). To assess whether miR-148a shows any effects on cell cycle, PMEks were stained by propidium iodide, and flow cytometric analysis revealed that the overexpression of miR-148a led to S-phase accumulation and prevented cells from progressing into the

G2/M phase compared with that of the controls (Figure 4c). Interestingly, this accumulation of cells in the S-phase suggests that miR-148a allows cells to commit to S-phase from G0/G1 but prevents progression through the cell cycle in KCs. Potentially acting as a checkpoint of mitosis from the S to the G2/M phase.

We next examined the effects of miR-148a during calcium-induced KC differentiation, which revealed a significant increase and/or decrease in expression at the transcript level of KC differentiation-associated genes (cytokeratin 1 [*K1*], *K10*, involucrin gene *Ivl*) after modulating miR-148a activities versus those of the controls (Figure 4d and e). In addition, *Rock1* and *Elf5* were also significantly increased and/or decreased in expression after modulation of miR-148a activities (Figure 4d and e). A similar impact on protein levels was observed after overexpression and/or inhibition of miR-148a for K1, Rock1, and Elf5 during KC differentiation (Figure 4f and g). We also attempted to determine whether miR-148a could prevent nuclear localization and activation of Rock1 and Elf5 on PMEks calcium-induced KC differentiation. Using immunocytochemistry and western blot analysis, we observed that Rock1 and Elf5 were significantly hindered in their ability to localize to the nucleus after the overexpression of miR-148a (pro-miR-148a) during differentiation (Supplementary Figure S4).

miRNA-148a regulates the expression of ROCK1 and ELF5 in skin and HFs

The expression of target genes as well as the impact on proliferation and differentiation were further examined in skin treated with anti-miR-148a in vivo (Figure 5). In the epidermis, inhibition of miR-148a resulted in increased and broader expression of K1 compared with that of the controls (Figure 5a and b). These data are consistent with our in vitro data showing miR-148a effects on KC differentiation (Figure 4d–g), suggesting that miR-148a is potentially required for maintaining skin integrity. However, we did not notice observable differences in Ki67 expression in miR-148a-inhibited (epidermis or HFs) compared with that of the controls (data not shown). These data suggest that loss of miR-148a in the epidermis can lead to the transition of KCs from proliferation to early differentiation in vivo.

We observed increased expression of Rock1 and Elf5 in the basal layer and appearance in suprabasal layers of treated skin with anti-miR-148a (Figure 5d and f) compared with that of the control epidermis (Figure 5c and e). In the HFs, Rock1 is increased in the discrete cell populations (outer root sheath, bulge, and hair bulb regions) in developing HFs (Figure 5d) compared with those in the control HFs (Figure 5c). Elf5 expression is observed throughout the HFs, including the developing hair bulb, outer root sheath, and bulge region (Figure 5f) compared with the expression in the control HFs, where expression was lower and restricted to the bulge region of HF and not present in advancing hair bulb (Figure 5e). These changes in expression were confirmed by quantitative immunofluorescence analysis, which revealed increased expression of K1, Rock1, and Elf5 in anti-miR-148a-treated versus in control skins (Figure 5g–i).

DISCUSSION

We have identified a previously undescribed role for miR-148a in the control of skin and HF maintenance and showed that (i) miR-148a shows spatiotemporal expression patterns predominately in the telogen stage of skin and HFs; (ii) the modulation of miR-148a in SCs and KCs affects cell proliferation, differentiation, and colony-forming abilities in vitro; (iii) inhibition of miR-148a during postnatal hair cycle results in HFs progressing further into anagen (without effecting HF morphology) and abnormal expression of differentiation and SCs markers and gene targets in vivo; and (iv) miR-148a regulates the balance of cellular processes in the skin and HFs by regulating the activities of two gene transcripts in the skin—Rock1 and Elf5—which are potentially required for normal development of skin and HFs. Our data suggest that miR-148a through its gene targets has an important regulatory role in these cellular programs controlling skin and hair cycle-associated changes of gene expressions. Our findings add miR-148a to only a few miRNAs reported in skin and HFs in regulating gene targets associated with stem/progenitor cells, proliferation, and differentiation during skin and HF development, homeostasis, and regeneration.

Analyzing the gene expression changes in primary KCs and showing that miR-148a is involved in regulating Rock1 and Elf5 in vitro and in vivo (Figures 3d–i and c–f) suggests that miR-148a acts, in part, by regulating the suprabasal expression of basal genes, thereby potentially acting as a switch between proliferation and differentiation in KCs.

miRNA-148a was also coexpressed with Rock1 and Elf5 in stem/progenitor cell regions of telogen HFs (bulge and hair germ) (Figure 3h and i), suggesting that miR-148a also has an important role in regulating SC fate and activity during HF cycling. Of note, miRNAs and their targets tend to be mutually exclusive in neighboring cells/tissues (Wang et al., 2019) as seen for miR-148a in the epidermis (basal vs. suprabasal). However, miRNA and target mRNA coexpression have also been observed in a cell- and tissue-dependent manner (Liu and Kohane, 2009), suggesting that a dual functionality of miR-148a is dependent on its spatiotemporal location in the skin. Our data suggest that miR-148a through Rock1 and Elf5 contributes to normal skin and HF development and homeostasis by finely regulating stem/progenitor cell activities leading to normal cell growth and homeostasis. However, currently, it is still unclear what functional roles Rock1 and Elf5 play within stem/progenitor cell populations in the skin and HFs, which require further investigations.

Subsequently, we observed that modulating miR-148a affects cellular proliferation and differentiation processes in vitro (Figure 4a–c). These findings are consistent with miR-148a's known function as an antiproliferative regulator, which is downregulated in cancer tissues, including the skin (Li et al., 2019; Wang et al., 2013b). Our data revealed cell accumulation at S phase–G2/M phase transition after

overexpression of miR-148a (Figure 4c). We speculate that this may be caused by the downregulation of *CDK1* and *CKS1β* because cell cycle arrest between S-phase and G2/M transition/mitosis has been attributed to impaired transcription of these genes (Martinsson-Ahlzén et al., 2008). In addition, CDK1 is a key regulator of S-phase and mitosis (Murray, 2004), whereas CKS1β promotes cell growth, invasion, and metastasis (Shi et al., 2020). Our data suggest that miR-148a is potentially regulating cell proliferation, in part, by controlling *CDK1* and *CKS1β* levels and contributes to a previously unreported mechanism of KC antiproliferative mitosis checkpoint to maintain healthy KCs.

During cellular differentiation, miR-148a has been shown to regulate skeletal muscle cell differentiation (Yin et al., 2020) and monocyte differentiation into macrophages (Huang et al., 2017). Of interest, inhibition of ROCK1 has been shown to result in the failure of human KCs to terminally differentiate (Chapman et al., 2014; McMullan et al., 2003), which is consistent with our data on PMEKs (Figure 4d–g), whereas ELF5 is essential in the control of mammary cell proliferation and differentiation processes (Zhou et al., 2005) and is expressed in differentiating KCs, inner root sheath, and outer root sheath layers of the HF (Choi et al., 2008; Singh et al., 2019). Our data suggest that in the epidermis, miR-148a may function, in part, by restricting the proliferative potential of stem/progenitors as they transitioned from basal to suprabasal layers through the regulation of Rock1 and Elf5 expression. This mechanism may explain how proliferating KCs commit to differentiation and how the epidermis is protected from cell growth abnormalities and disease.

We next examined the longer-term effects in vivo by inhibiting miR-148a in postnatal skin and hair cycle-associated tissue remodeling. We observed that the inhibitory effects of miR-148a lead to telogen–anagen progression, modulation of stem/progenitor activities, and differentiation processes (Figures 2 and 5) but not to proliferation in vivo. These data suggest that miR-148a is an important regulator of HF progression (telogen to anagen transition) through tight regulation of HF stem/progenitor cell populations. Our findings suggest that negative regulation of Rock1 by miR-148a may maintain the self-renewal and stemness characteristics of HF SCs, which have been observed in primary skin tissue cultures after inhibition of ROCK1 (An et al., 2018). In addition, studies have suggested that ROCK1 signaling inhibition elevates stem/progenitor cell functions, in vitro (Centonze et al., 2022). Furthermore, ROCK1 has been shown to promote embryonic SC colony formation and maintenance of neural progenitor cells (Chang et al., 2010), whereas Elf5 is expressed in differentiated epidermal and oral mouse KCs as well as in the inner root sheath and outer root sheath of HFs (Choi et al., 2008; Oakes et al., 2008; Parikh et al., 2008; Singh et al., 2019; Tummala and Sinha, 2006). However, Elf5's functional role in these cell populations has not been determined. It is therefore important to understand

basal layer (panel h, arrow). Negative controls are included in Supplementary Figure S3 (Supplementary Materials and Methods). The broken lines demarcate the epidermal–dermal border. The dotted box denotes the area that has been magnified (right side panels). * $P < 0.05$, ** $P < 0.01$, and *** $P < 0.001$ with Student's *t*-test. Bars = 50 μm (h and i) and 25 μm (h and i for the right side panels). PMEK, primary mouse epidermal keratinocyte; SHG, secondary hair germ; UTR, untranslated region.

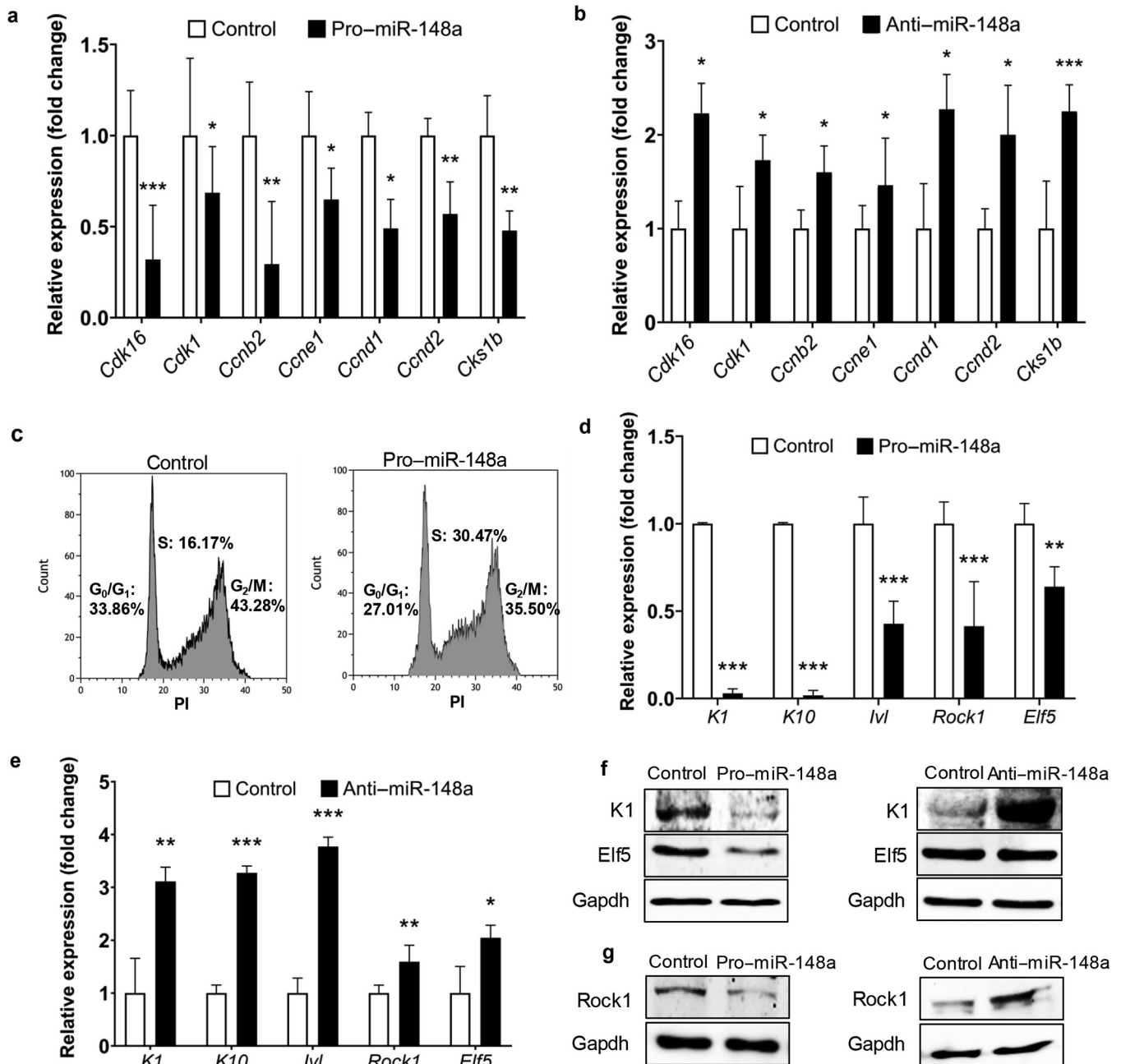


Figure 4. miRNA-148a regulates keratinocyte proliferation and differentiation. (a, b) RT-qPCR analysis of cell cycle gene markers in PMEKs showed an increase and/or decrease in the expression of genes analyzed after modulation of miR-148a activities, respectively. Data are presented as mean \pm SEM values from three independent experiments. (c) Flow cytometric analysis by PI in PMEKs showed accumulation in S-phase and, subsequently, a reduction of cells entering the G₂/M phase of the cell cycle after miR-148a overexpression (pro-miR-148a). The graphs shown are from a single representative experiment. Percentages are presented as mean values from three independent experiments. (d, e) RT-qPCR analysis during calcium-induced (1.8 mM) keratinocyte differentiation in PMEKs showing an increase and/or decrease in the expression of keratinocyte differentiation-associated markers cyokeratin 1 (*K1*), *K10*, and involucrin (*Ivl*) and gene targets *Rock1* and *Elf5* after modulating miR-148a activity, respectively. Data are presented as mean \pm SEM values from three independent experiments. (f, g) Western blot analysis of *K1*, *Rock1*, and *Elf5* during calcium-induced keratinocyte differentiation in PMEKs: overexpression of miR-148a reduces the expression of *K1*, *Rock1*, and *Elf5*, whereas anti-miR-148a (inhibition) leads to an increase in protein levels. Data shown are from a single representative experiment of three experimental repeats. * $P < 0.05$, ** $P < 0.01$, and *** $P < 0.001$ with Student's *t*-test. *K1*, keratin 1; PI, propidium iodide; PMEK, primary mouse epidermal keratinocyte.

the expression pattern of *Elf5* to explore its potential functions in skin and HFs. We believe that *Elf5* (through miR-148a regulation) may have a similar functional role, as determined in other epithelial tissues (Chakrabarti et al., 2012; Grassmeyer et al., 2017; Zhou et al., 2005), in regulating

stem/progenitor cells and cell fate processes in skin and HFs, which require further investigations.

In the epidermis, miR-148a can regulate the transition of KCs from proliferation to early differentiation, at least in part, through the modulation of the activity and expression of

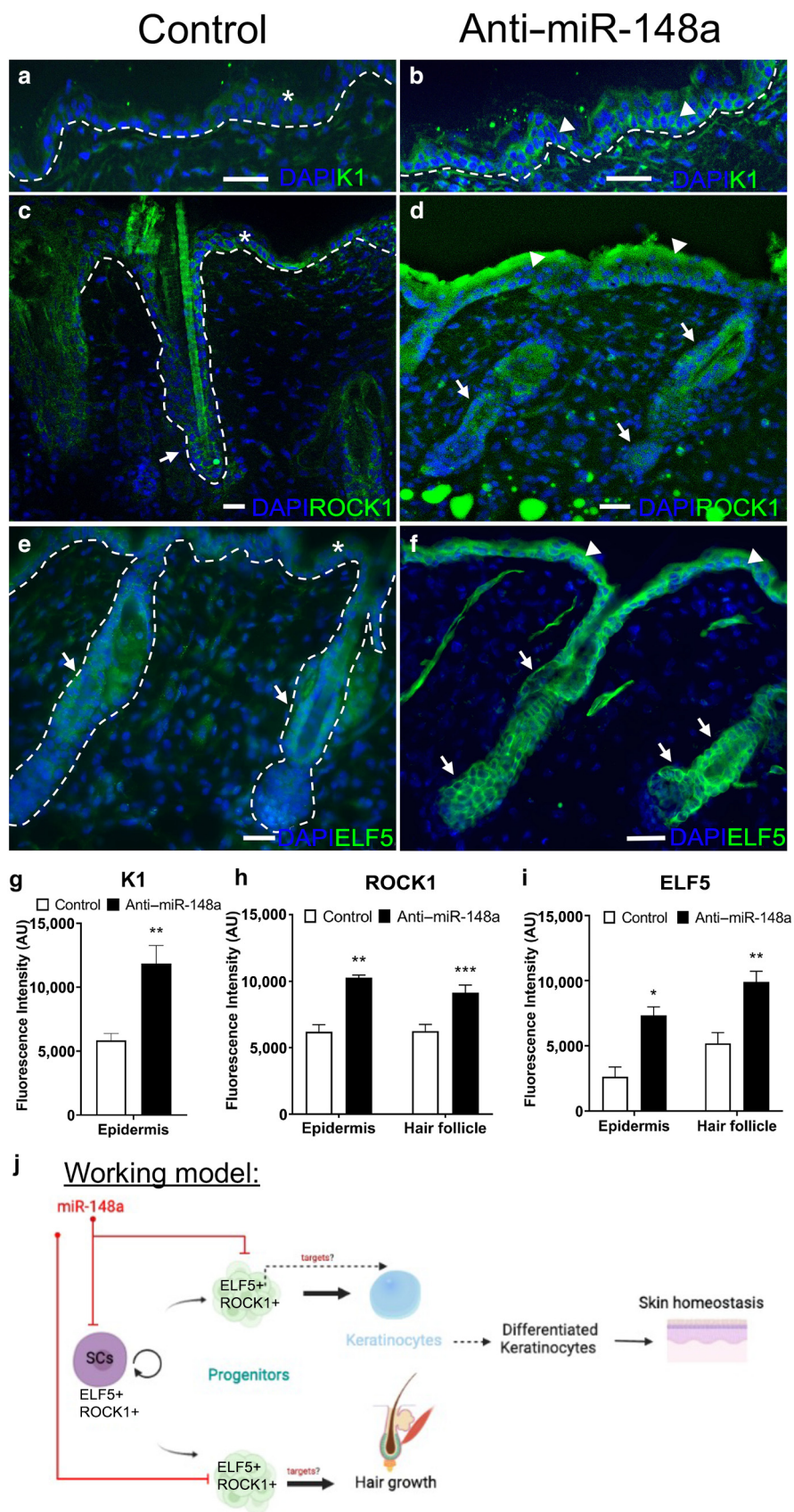


Figure 5. Inhibition of miRNA-148a leads to elevated expression of ROCK1 and ELF5 in skin and hair follicles. Anti-miR-148a (inhibition) or miRIDIAN-negative controls were administered daily subcutaneously at postnatal skin days P20–P22. The skin was harvested at P23. (a–c) Representative microphotographs of control and anti-miR-148a-treated mice sections: immunohistochemistry staining for cytokeratin 1 (K1), Rock1 (green), Elf5 (green), and DAPI (blue) of skin sections. K1 immunohistochemistry in the epidermis: increased expression of K1 in the basal layer after anti-miR-148a treatment (panel b,

Rock1 and Elf5, which are required to maintain healthy skin and HFs. ROCK1 has been shown to be involved in the proliferation and differentiation processes of KCs and in other epithelial cells (Ma et al., 2017). In addition, reduced ROCK1 function results in cellular senescence, both in vitro and in vivo (Centonze et al., 2022; Kümper et al., 2016). This loss of ROCK1-mediated cellular senescence involves the downregulation of cell cycle protein CDK1 (Diril et al., 2012). Of note, after modulating miR-148a expression, we observed that Cdk1 along with Rock1 was upregulated and/or downregulated in PMEks (Figure 4a and b). Our data suggest that miR-148a may regulate KC proliferation and differentiation in the skin by regulating cell cycle progression either by targeting *CDK1* directly (Wang et al., 2020) or through the downregulation of Rock1, leading to reduced *CDK1* (Kümper et al., 2016) or both in KCs. Interestingly, elevated ROCK1 expression has also been implicated in tumor progression, deregulated differentiation, expansion of SC populations, and increased motility in KCs (Benitah et al., 2004; Lefort et al., 2007; Whatcott et al., 2017; Wilkinson et al., 2005). This suggests that miR-148a regulation of Rock1 may also prevent cancer formation in the skin, which is consistent with its role as a tumor suppressor. These data highlight a potential previously unknown role of miR-148a as a protector against age-related pathological conditions, such as cellular senescence, as well as a previously undescribed mechanism of antitumorigenic function through Rock1, leading to the control of normal cell proliferation and differentiation processes in the skin.

In summary, our data reveal that miR-148a is a key determinant that controls the activities of Rock1 and Elf5 in the skin. Because both Rock1 and Elf5 play crucial roles in the control of cellular proliferation and differentiation and stem/progenitor cell activity in many organs, we propose that an essential function of miR-148a in the epidermis is to restrict the proliferative potential of basal cell progenitors as they transitioned from basal to suprabasal layers. Although in HFs, miR-148a role also serves to regulate SC fate and activity, in part, by regulating Rock1 and Elf5 during HF development/homeostasis and cycling (Figure 5j). These data provide an important foundation for further analyses of the role of miR-148a as a regulator of pathway activities in many areas of research, including SC and cancer biology, regenerative medicine, and aging. Our findings also provide compelling evidence that miR-148a represents a potentially powerful candidate therapeutic target, which requires further exploration.

MATERIAL AND METHODS

Animals

Animal studies were performed in accordance with protocols approved by the UK Home Office Project License. C57Bl/6 WT female mice were purchased from Charles River Laboratories (Wilmington, MA). Skin samples were collected at defined stages during hair cycle-associated tissue remodeling (Müller-Röver et al., 2001) and snap frozen in liquid nitrogen for histological, immunofluorescent, and RT-qPCR analysis. Skin samples were taken during postnatal hair cycle days 12–23, and the hair cycle was induced as described previously (Mardaryev et al., 2010) and harvested at days 0–19 after depilation for in situ hybridization and RT-qPCR analysis.

Cell culture and transfection

Cell culture and transfections of PMEks were prepared from C57Bl/6 WT newborn mice at postnatal days 2–3, as described previously (Ahmed et al., 2014), and grown at 33 °C in 8% carbon dioxide until 60–70% confluent. PMEks were transfected with 200 nM synthetic miR-148a mimic (pro-miR-148a), miR-148a inhibitor (anti-miR-148), or miRNA-negative controls (Thermo Fisher Scientific, Horsham, United Kingdom) using Lipofectamine 3000 (Thermo Fisher Scientific) as done previously (Ahmed et al., 2019).

RNA-sequencing analysis

PMEks were cultured and transfected with pro-miR-148a and miRNA control, and RNA was extracted as described in Supplementary Materials and Methods. Samples were sent to Novogene (Cambridge, United Kingdom) for RNA sequencing using Illumina Novoseq 6000 platform. The sequencing data were uploaded to the Galaxy web platform, and we used the public server at <https://usegalaxy.org/> to analyze the data as described previously (Afgan et al., 2016). The sequenced data were aligned to mus musculus genome (*Mm9*). Genes that were insignificantly changed ($P > 0.05$) were excluded from our analysis. Gene ontology analysis and heat maps were generated using Galaxy web platform.

Pharmacological treatment of skin

Pharmacological treatment of mice with anti-miR-148a was performed as described previously (Mardaryev et al., 2010). In brief, synthetic miR-148a inhibitor (anti-miR-148a) or miRIDIAN-negative control (Thermo Fisher Scientific) was administered subcutaneously to the dorsal skin of C57Bl/6 WT mice at a concentration of 20 μM using atelocollagen (Koken, Tokyo, Japan) for their local and sustained delivery. Anti-miR-148a treatment was performed on postnatal skin days 20, 21, and 22, and skin samples were collected on postnatal day 23. In each experiment, ≥3 or 4 mice per time point were used for analyses in both experimental and control groups. Collected samples were processed for histological, immunofluorescent, and RT-qPCR analysis.

arrowheads), compared with that of the control skins (panel a, asterisk). Immunohistochemistry staining of Rock1 and Elf5: increased expression was observed for Rock1 in the epidermis (panel d, arrowheads) compared with that of the controls (panel c, asterisk). In the HFs, Rock1 is elevated in the distinct cell populations (ORS, bulge, and hair bulb regions) (panel d, arrows) compared with that in the control HFs (panel c, arrows). Elf5 expression was elevated in both the basal and suprabasal layers of the epidermis (panel f, arrowheads) compared with that in the control skins (panel e, asterisk). In the HFs, Elf5 expression is elevated in the hair bulb, ORS, and bulge regions (panel f, arrows) compared with that in the control HFs where expression was restricted to the bulge region (panel e, arrows). The broken lines demarcate the epidermal–dermal border. (g–i) Quantitative immunofluorescence analysis: immunodetection of (g) K1, (h) Rock1, and (i) Elf5 in the epidermis and HFs (green fluorescence) of control versus anti-miR-148a-treated skin samples normalized to DAPI⁺ cells. $n = 3$ mice per treatment. Data are presented as mean ± SEM (error bars). (j) A working model of the involvement of miR-148a in the regulation of skin and HF stem cells and their lineage-committed progenies that controls skin and HF development and homeostasis through its gene targets Rock1 and Elf5. These effects may also be linked to the activation/repression of specific signaling pathways in keratinocytes that result from the regulation of Rock1 and Elf5 by miR-148a, which are yet to be determined (created with BioRender.com). Bars = 50 μm. . P denotes postnatal day. Au, arbitrary unit; HF, hair follicle; K, keratin; ORS, outer root sheath.

FACS

Skins from C57Bl/6 WT mice were harvested between ages 7 and 9 weeks. In brief, dissected and minced tissue was filtered using a 40- μ m filter. The cells were centrifuged down at 300g for 10 minutes and resuspended in 1 ml of EMEM calcium-free medium (Lonza, Manchester, United Kingdom). Cells were stained with Ly-6A/E (SCA-1) (Thermo Fisher Scientific), CD34 (RAM34) (Thermo Fisher Scientific), and CD49f (BD Pharmingen, San Diego, CA) in a 2% BSA/PBS staining buffer rotating for 1 hour at 4 °C. Cells were then stained with secondary antibody allophycocyanin streptavidin (BioLegend, San Diego, CA) for 1 hour at 4 °C. CD34⁺/CD49f^{high}/SCA-1⁻ HF-bulge SCs, CD34⁻/CD49f^{high}/SCA-1⁺ basal SCs, and CD34⁻/CD49f^{low}/SCA-1⁻ suprabasal KCs were sorted using a MoFlo-XDP cell sorter (Beckman Coulter, High Wycombe, United Kingdom), and data were analyzed using Summit software (Beckman Coulter). Sorted SCs were then used for subsequent colony-forming assays and RT-qPCR analysis.

Colony-forming assay

Swiss-3T3 cells were grown in DMEM media (Thermo Fisher Scientific) in 24-well plates at 37 °C with 5% carbon dioxide. At 70% confluence, 3T3 cells were treated with 8 μ g/ml mitomycin C (Thermo Fisher Scientific) for 2 hours. A total of 1,000 HF-bulge SCs were seeded per 24-well plate and incubated for 48 hours with DMEM/F-12 media (3:1) supplemented with 10% chelated fetal bovine serum, 10 ng/ml epidermal GF, 0.5 μ g/ml hydrocortisone, 10⁻¹⁰ M cholera toxin, 5 μ g/ml insulin, 1.8⁻⁴ M Adenine (Merck, Feltham, United Kingdom), 100 U/ml penicillin, 100 μ g/ml streptomycin, and 0.3 mM calcium. Forty-eight hours after seeding, SCs were transduced with MiRZIP-148a or short hairpin RNA control lentiviruses at a multiplicity of infection of 20 (4.0 \times 10⁴ viral titer/ml) supplemented with 8 μ g/ml polybrene (Thermo Fisher Scientific) for 4 hours at 32 °C with 5% carbon dioxide. Media was replaced every 48 hours and cultured for 10 days. GFP and phase imaging were performed using IncuCyte S3 live cell analysis instrument (Sartorius Stedim Biotech, Göttingen, Germany).

Data and code availability

The data that support the findings of this study are openly available in Gene Expression Omnibus Datasets at <https://www.ncbi.nlm.nih.gov/gds>, reference number GSE197862.

ORCID

Maximillian E. Pickup: <http://orcid.org/0000-0002-6006-2540>
 Anhua Hu: <http://orcid.org/0000-0001-8821-6591>
 Hetal J. Patel: <http://orcid.org/0000-0002-8461-9980>
 Mohammed I. Ahmed: <http://orcid.org/0000-0002-9051-7681>

CONFLICT OF INTEREST

The authors state no conflict of interest.

ACKNOWLEDGMENTS

This work was supported by funding from Nottingham Trent University (Nottingham, United Kingdom) (UoA03 QR and Capital Funds [MIA]). The Leica Thunder Imager 3D Cell Culture was obtained using funds provided by the Office for Students. We would like to thank Natalia Botchkareva for her critical comments on the manuscript. We would also like to thank Stephen Reed (FACS), Graham Hickman (Microscopy), and Andrew Marr and his team (Biological Services animal unit) for their support and expertise.

AUTHOR CONTRIBUTIONS

Conceptualization: MIA; Data Curation: MEP, AH, HJP, MIA; Formal Analysis: MEP, MIA; Funding Acquisition: MIA; Writing – Original Draft Preparation: MIA.

SUPPLEMENTARY MATERIAL

Supplementary material is linked to the online version of the paper at www.jidonline.org, and at <https://doi.org/10.1016/j.jid.2022.06.028>

REFERENCES

- Afgan E, Baker D, van den Beek M, Blankenberg D, Bouvier D, Čech M, et al. The Galaxy platform for accessible, reproducible and collaborative biomedical analyses: 2016 update. *Nucleic Acids Res* 2016;44:W3–10.
- Ahmed MI, Alam M, Emelianov VU, Poterlowicz K, Patel A, Sharov AA, et al. MicroRNA-214 controls skin and hair follicle development by modulating the activity of the Wnt pathway. *J Cell Biol* 2014;207:549–67.
- Ahmed MI, Mardaryev AN, Lewis CJ, Sharov AA, Botchkareva NV. MicroRNA-21 is an important downstream component of BMP signalling in epidermal keratinocytes. *J Cell Sci* 2011;124:3399–404.
- Ahmed MI, Pickup ME, Rimmer AG, Alam M, Mardaryev AN, Poterlowicz K, et al. Interplay of MicroRNA-21 and SATB1 in epidermal keratinocytes during skin aging. *J Invest Dermatol* 2019;139:2538–42.e2.
- Ambros V. microRNAs: tiny regulators with great potential. *Cell* 2001;107:823–6.
- An L, Ling P, Cui J, Wang J, Zhu X, Liu J, et al. ROCK inhibitor Y-27632 maintains the propagation and characteristics of hair follicle stem cells. *Am J Transl Res* 2018;10:3689–700.
- Andl T, Murchison EP, Liu F, Zhang Y, Yunta-Gonzalez M, Tobias JW, et al. The miRNA-processing enzyme dicer is essential for the morphogenesis and maintenance of hair follicles. *Curr Biol* 2006;16:1041–9.
- Aunin E, Bradley D, Ahmed MI, Mardaryev AN, Botchkareva NV. Exploring a role for regulatory miRNAs in wound healing during ageing: involvement of miR-200c in wound repair. *Sci Rep* 2017;7:3257.
- Benitah SA, Valerón PF, van Aelst L, Marshall CJ, Lacal JC. Rho GTPases in human cancer: an unresolved link to upstream and downstream transcriptional regulation. *Biochim Biophys Acta* 2004;1705:121–32.
- Blanpain C, Fuchs E. Epidermal homeostasis: a balancing act of stem cells in the skin. *Nat Rev Mol Cell Biol* 2009;10:207–17.
- Blanpain C, Lowry WE, Geoghegan A, Polak L, Fuchs E. Self-renewal, multipotency, and the existence of two cell populations within an epithelial stem cell niche. *Cell* 2004;118:635–48.
- Centonze G, Centonze S, Ponzone L, Calautti E. ROCK 'n TOR: an Outlook on keratinocyte Stem Cell Expansion in Regenerative Medicine via protein kinase Inhibition. *Cells* 2022;11:1130.
- Chakrabarti R, Wei Y, Romano RA, DeCoste C, Kang Y, Sinha S. Elf5 regulates mammary gland stem/progenitor cell fate by influencing notch signaling. *Stem Cells (Dayt Ohio)* 2012;30:1496–508.
- Chang TC, Chen YC, Yang MH, Chen CH, Hsing EW, Ko BS, et al. Rho kinases regulate the renewal and neural differentiation of embryonic stem cells in a cell plating density-dependent manner. *PLoS One* 2010;5:e9187.
- Chapman S, McDermott DH, Shen K, Jang MK, McBride AA. The effect of Rho kinase inhibition on long-term keratinocyte proliferation is rapid and conditional. *Stem Cell Res Ther* 2014;5:60.
- Choi YS, Cheng J, Segre J, Sinha S. Generation and analysis of Elf5-LacZ mouse: unique and dynamic expression of Elf5 (ESE-2) in the inner root sheath of cycling hair follicles. *Histochem Cell Biol* 2008;129:85–94.
- Diril MK, Ratnacaram CK, Padmakumar VC, Du T, Wasser M, Coppola V, et al. Cyclin-dependent kinase 1 (Cdk1) is essential for cell division and suppression of DNA re-replication but not for liver regeneration. *Proc Natl Acad Sci USA* 2012;109:3826–31.
- Grassmeyer J, Mukherjee M, deRiso J, Hettinger C, Bailey M, Sinha S, et al. Elf5 is a principal cell lineage specific transcription factor in the kidney that contributes to Aqp2 and Avpr2 gene expression. *Dev Biol* 2017;424:77–89.
- Hansen LS, Coggle JE, Wells J, Charles MW. The influence of the hair cycle on the thickness of mouse skin. *Anat Rec* 1984;210:569–73.
- Hsu YC, Li L, Fuchs E. Emerging interactions between skin stem cells and their niches. *Nat Med* 2014;20:847–56.
- Huang F, Zhao JL, Wang L, Gao CC, Liang SQ, An DJ, et al. miR-148a-3p mediates notch signaling to promote the differentiation and M1 activation of macrophages. *Front Immunol* 2017;8:1327.
- Inui M, Martello G, Piccolo S. MicroRNA control of signal transduction. *Nat Rev Mol Cell Biol* 2010;11:252–63.

- Kümper S, Mardakheh FK, McCarthy A, Yeo M, Stamp GW, Paul A, et al. Rho-associated kinase (ROCK) function is essential for cell cycle progression, senescence and tumorigenesis. *eLife* 2016;5:e12994.
- Lee RC, Feinbaum RL, Ambros V. The *C. elegans* heterochronic gene *lin-4* encodes small RNAs with antisense complementarity to *lin-14*. *Cell* 1993;75:843–54.
- Lefort K, Mandinova A, Ostano P, Kolev V, Calpini V, Kolfschoten I, et al. Notch1 is a p53 target gene involved in human keratinocyte tumor suppression through negative regulation of ROCK1/2 and MRCK α kinases. *Genes Dev* 2007;21:562–77.
- Lena AM, Shalom-Feuerstein R, Rivetti di Val Cervo PR, Aberdam D, Knight RA, Melino G, et al. miR-203 represses 'stemness' by repressing deltaNp63. *Cell Death Differ* 2008;15:1187–95.
- Li Y, Li W, Zeng X, Tang X, Zhang S, Zhong F, et al. The role of microRNA-148a and downstream DLGAP1 on the molecular regulation and tumor progression on human glioblastoma. *Oncogene* 2019;38:7234–48.
- Liu H, Kohane IS. Tissue and process specific microRNA–mRNA co-expression in mammalian development and malignancy. *PLoS One* 2009;4:e5436.
- Luo Q, Li W, Zhao T, Tian X, Liu Y, Zhang X. Role of miR-148a in cutaneous squamous cell carcinoma by repression of MAPK pathway. *Arch Biochem Biophys* 2015;583:47–54.
- Ma D, Xie D, Chu YL, Li C, Chen M, Zhang L, et al. RhoA / ROCK 1 signaling pathway is involved in proliferation and differentiation in human lung fibroblast cells. *Int J Clin Exp Pathol* 2017;10:6170–8.
- Mardaryev AN, Ahmed MI, Vlahov NV, Fessing MY, Gill JH, Sharov AA, et al. Micro-RNA-31 controls hair cycle-associated changes in gene expression programs of the skin and hair follicle. *FASEB J* 2010;24:3869–81.
- Martinsson-Ahlzén HS, Liberal V, Grünenfelder B, Chaves SR, Spruck CH, Reed SI. Cyclin-dependent kinase-associated proteins Cks1 and Cks2 are essential during early embryogenesis and for cell cycle progression in somatic cells. *Mol Cell Biol* 2008;28:5698–709.
- McMullan R, Lax S, Robertson VH, Radford DJ, Broad S, Watt FM, et al. Keratinocyte differentiation is regulated by the Rho and ROCK signaling pathway. *Curr Biol* 2003;13:2185–9.
- Müller-Röver S, Handjiski B, van der Veen C, Eichmüller S, Foitzik K, McKay IA, et al. A comprehensive guide for the accurate classification of murine hair follicles in distinct hair cycle stages. *J Invest Dermatol* 2001;117:3–15.
- Murray AW. Recycling the cell cycle: cyclins revisited. *Cell* 2004;116:221–34.
- Oakes SR, Naylor MJ, Asselin-Labat ML, Blazek KD, Gardiner-Garden M, Hilton HN, et al. The Ets transcription factor Elf5 specifies mammary alveolar cell fate. *Genes Dev* 2008;22:581–6.
- O'Brien J, Hayder H, Zayed Y, Peng C. Overview of microRNA biogenesis, mechanisms of actions, and circulation. *Front Endocrinol (Lausanne)* 2018;9:402.
- Parikh N, Nagarajan P, Sei-Ichi M, Sinha S, Garrett-Sinha LA. Isolation and characterization of an immortalized oral keratinocyte cell line of mouse origin. *Arch Oral Biol* 2008;53:1091–100.
- Pong SK, Gullerova M. Noncanonical functions of microRNA pathway enzymes – drosha, DGCR8, Dicer and Ago proteins. *FEBS Lett* 2018;592:2973–86.
- Shi W, Huang Q, Xie J, Wang H, Yu X, Zhou Y. CKS1B as drug resistance-inducing gene-a potential target to improve cancer therapy. *Front Oncol* 2020;10:582451.
- Singh S, Elenio E, Leu NA, Romano RA, Vaughan AE, DeRiso J, et al. A new Elf5^{CreERT2-GFP} BAC transgenic mouse model for tracing Elf5 cell lineages in adult tissues. *FEBS Lett* 2019;593:1030–9.
- Takahashi M, Cuatrecasas M, Balaguer F, Hur K, Toiyama Y, Castells A, et al. The clinical significance of MiR-148a as a predictive biomarker in patients with advanced colorectal cancer. *PLoS One* 2012;7:e46684.
- Teta M, Choi YS, Okegbe T, Wong G, Tam OH, Chong MMW, et al. Inducible deletion of epidermal Dicer and Drosha reveals multiple functions for miRNAs in postnatal skin. *Development* 2012;139:1405–16.
- Tian Y, Wei W, Li L, Yang R. Down-regulation of miR-148a promotes metastasis by DNA methylation and is associated with prognosis of skin cancer by targeting TGIF2. *Med Sci Monit* 2015;21:3798–805.
- Trempus CS, Morris RJ, Bortner CD, Cotsarelis G, Faircloth RS, Reece JM, et al. Enrichment for living murine keratinocytes from the hair follicle bulge with the cell surface marker CD34. *J Invest Dermatol* 2003;120:501–11.
- Tummala R, Sinha S. Differentiation-specific transcriptional regulation of the ESE-2 gene by a novel keratinocyte-restricted factor. *J Cell Biochem* 2006;97:766–81.
- Wang C, Shao S, Deng L, Wang S, Zhang Y. LncRNA SNHG12 regulates the radiosensitivity of cervical cancer through the miR-148a/CDK1 pathway. *Cancer Cell Int* 2020;20:554.
- Wang D, Zhang Z, O'Loughlin E, Wang L, Fan X, Lai EC, et al. MicroRNA-205 controls neonatal expansion of skin stem cells by modulating the PI(3)K pathway. *Nat Cell Biol* 2013a;15:1153–63.
- Wang N, Zheng J, Chen Z, Liu Y, Dura B, Kwak M, et al. Single-cell microRNA-mRNA co-sequencing reveals non-genetic heterogeneity and mechanisms of microRNA regulation. *Nat Commun* 2019;10:95.
- Wang SH, Li X, Zhou LS, Cao ZW, Shi C, Zhou CZ, et al. microRNA-148a suppresses human gastric cancer cell metastasis by reversing epithelial-to-mesenchymal transition. *Tumour Biol* 2013b;34:3705–12.
- Whatcott CJ, Ng S, Barrett MT, Hostetter G, Von Hoff DD, Han H. Inhibition of ROCK1 kinase modulates both tumor cells and stromal fibroblasts in pancreatic cancer. *PLoS One* 2017;12:e0183871.
- Wilkinson S, Paterson HF, Marshall CJ. Cdc42–MRCK and Rho–ROCK signalling cooperate in myosin phosphorylation and cell invasion. *Nat Cell Biol* 2005;7:255–61.
- Yi R, O'Carroll D, Pasolli HA, Zhang Z, Dietrich FS, Tarakhovskiy A, et al. Morphogenesis in skin is governed by discrete sets of differentially expressed microRNAs. *Nat Genet* 2006;38:356–62.
- Yi R, Pasolli HA, Landthaler M, Hafner M, Ojo T, Sheridan R, et al. DGCR8-dependent microRNA biogenesis is essential for skin development. *Proc Natl Acad Sci USA* 2009;106:498–502.
- Yi R, Poy MN, Stoffel M, Fuchs E. A skin microRNA promotes differentiation by repressing 'stemness'. *Nature* 2008;452:225–9.
- Yin H, He H, Cao X, Shen X, Han S, Cui C, et al. MiR-148a-3p regulates skeletal muscle satellite cell differentiation and apoptosis via the PI3K/AKT signaling pathway by targeting Meox2. *Front Genet* 2020;11:512.
- Zhang L, Stokes N, Polak L, Fuchs E. Specific microRNAs are preferentially expressed by skin stem cells to balance self-renewal and early lineage commitment. *Cell Stem Cell* 2011;8:294–308.
- Zhao B, Chen Y, Yang N, Chen Q, Bao Z, Liu M, et al. miR-218-5p regulates skin and hair follicle development through Wnt/ β -catenin signaling pathway by targeting SFRP2. *J Cell Physiol* 2019;234:20329–41.
- Zhou J, Chehab R, Tkalcevic J, Naylor MJ, Harris J, Wilson TJ, et al. Elf5 is essential for early embryogenesis and mammary gland development during pregnancy and lactation. *EMBO J* 2005;24:635–44.



This work is licensed under a Creative Commons Attribution-NonCommercial-NoDerivatives 4.0 International License. To view a copy of this license, visit <http://creativecommons.org/licenses/by-nc-nd/4.0/>

SUPPLEMENTARY MATERIALS AND METHODS

Cell culture and transfection

Cell culture and transfections of primary mouse epidermal keratinocytes (PMEKs) were prepared from C57Bl/6 wild-type newborn mice at postnatal days 2–3 as described previously (Ahmed et al., 2014). In brief, PMEKs were grown in EMEM calcium-free medium (Lonza, Manchester, United Kingdom) supplemented with 0.05 mM calcium (Thermo Fisher Scientific, Horsham, United Kingdom), 4% chelated heat-inactivated fetal bovine serum (Thermo Fisher Scientific), 0.4 µg/ml hydrocortisone (Merck, Feltham, United Kingdom), 5 µg/ml insulin (Merck), 10 ng/ml epidermal GF (Merck), 10^{-10} M cholera toxin (Merck), 2×10^{-9} M T3 (Merck), 100 U/ml penicillin (Thermo Fisher Scientific), 100 µg/ml streptomycin (Thermo Fisher Scientific), and 2 mM L-glutamine (Thermo Fisher Scientific) at 33 °C with 8% carbon dioxide until 60–70% confluent. PMEKs were transfected with 200 nM of synthetic miR-148a mimic (pro-miR-148a), miR-148a inhibitor (anti-miR-148), or miRNA-negative controls (Thermo Fisher Scientific) using Lipofectamine 3000 (Thermo Fisher Scientific) as done previously (Ahmed et al., 2019). Cells were harvested 48 hours after transfection and used for further analyses. For calcium-induced keratinocyte differentiation analysis, PMEKs were differentiated after transfection by media supplementation with 1.8 mM calcium. PMEKs were cultured for an additional 48 hours after transfection before collection for further analysis.

Reverse Transcription Quantitative Real-Time PCR (RT-qPCR)

Total RNA was isolated using the Zymo Direct-zol RNA kit (Cambridge Biosciences, Cambridge, United Kingdom). For gene expression analysis, 100 ng of total RNA was converted into cDNA using the qPCRBIO cDNA Synthesis Kit system (PCR Biosystems, London, United Kingdom). Gene expression analysis was performed on QuantStudio5 Real-Time PCR System (Thermo Fisher Scientific). Gene expression was analyzed using qPCRBIO SyGreen mix (PCR Biosystems) under the following conditions: 95 °C for 2 minutes, followed by 40 cycles of denaturation (95 °C for 5 seconds) and annealing and extension (30 seconds at temperature experimentally determined for each primer pair). RT-qPCR primers (Supplementary Table S1) were designed using primer3 (<https://primer3.ut.ee/>) and further validated using the University of California Santa Cruz genome browser (<https://genome.ucsc.edu/>) and National Center for Biotechnology Information primer blast (<https://www.ncbi.nlm.nih.gov/tools/primer-blast/>). Amplification differences between samples and controls were calculated on the basis of the Ct ($\Delta\Delta$ Ct) method and normalized to mouse *Actin* gene (*Actb*). Data from triplicates were pooled, \pm SEM was calculated, and statistical analysis was performed using unpaired student's *t*-test.

For detection of miR-148a, TaqMan quantitative reverse transcriptase PCR was performed using TaqMan Real-Time PCR Assay (Thermo Fisher Scientific) as described previously (Ahmed et al., 2019, 2014). In brief, miR-148a was amplified under the following cycling conditions: 95 °C for 10 minutes, followed by 40 cycles of 95 °C for 15 seconds and 60 °C for 60 seconds. Differences between samples and

controls were calculated on the basis of the Ct ($\Delta\Delta$ Ct) method and normalized to the U6 small nuclear RNA values. Data from triplicates were pooled, \pm SEM was calculated, and statistical analysis was performed using unpaired Student's *t*-test.

Western blot

Whole-cell protein lysates were extracted from cultured cells using RIPA lysis buffer (50 mM Tris-hydrogen chloride, 1% NP-40, 0.25% sodium deoxycholate, 150 mM sodium chloride, and 1 mM EDTA; pH 7.4) and cOmplete ULTRA Protease Inhibitor Cocktail (Merck). Nuclear protein was extracted from cultured cells using NE-PER Nuclear and Cytoplasmic extraction kit (Thermo Fisher Scientific). Western blot was performed as described previously (Ahmed et al., 2019). In brief, 10 µg of protein were processed for western blot analysis, followed by membrane incubation with primary antibody (Supplementary Table S2) overnight at 4 °C. Horseradish peroxidase-tagged IgG antibodies were used as secondary antibodies (1:3,000, Thermo Fisher Scientific). Antibody binding was visualized with an enhanced chemiluminescence system (SuperSignal West Pico Kit, Thermo Fisher Scientific) on the FL1000 iBright GelDoc Imager (Thermo Fisher Scientific).

Flow cytometry

PMEKs were cultured and transfected with pro-miR-148a or miRNA control as described earlier. Forty-eight hours after transfection, cells were trypsinized, washed, and fixed in 70% ethanol/PBS at –20 °C for 30 minutes. Fixed cells were incubated with RNase A (100 µg/ml) for 30 minutes at 37 °C. Cells were subsequently incubated with 20 µg/ml propidium iodide (Thermo Fisher Scientific) for 30 minutes at 4 °C. The percentage of cells at distinct phases of the cell cycle was analyzed by flow cytometry with a Beckman Coulter Gallios (Beckman Coulter, High Wycombe, United Kingdom). For each sample, 10,000 events were collected and analyzed on Beckman Coulter Kaluza Analysis Software (Beckman Coulter).

In situ hybridization and FISH

In situ hybridization was performed as described previously (Pickup and Ahmed, 2020). In brief, skin cryosections (10 µm) were fixed in 4% paraformaldehyde (Thermo Fisher Scientific) for 10 minutes at room temperature. Slides were hybridized with 320 nM double-DIG-labeled miR-148a probe (Qiagen, Germantown, MD) diluted in hybridization buffer (50% formamide DI (Merck), 5× saline-sodium citrate (Thermo Fisher Scientific), 50 µg/ml yeast RNA (Thermo Fisher Scientific), 1% SDS (Thermo Fisher Scientific), and 50 µg/ml heparin (Thermo Fisher Scientific) for 16–18 hours at 60 °C overnight. Slides were subsequently washed and blocked for 60 minutes in blocking solution (2% blocking reagent, Merck), 5% heat-inactivated sheep serum (Merck), 1% Tween-20, and levamisole in 1× Tris-buffered saline 0.1% Tween 20. Slides were incubated for 2 hours at room temperature with sheep alkaline phosphatase-conjugated anti-DIG antibody (1:2,500, Merck).

FISH was performed with the following modifications. Slides were blocked for 30 minutes in blocking solution (0.1 M Tris-hydrogen chloride [pH 7.5], 0.15 M sodium chloride,

and 0.5% blocking reagent, Merck). Immunodetection of miR-148a was performed with sheep rhodamine-conjugated anti-DIG antibody (1:100, Merck) alongside antibodies for ROCK1, ELF5, CD34, or keratin 15 (Supplementary Table S2). Slides were incubated overnight at 4 °C. Slides were then washed and incubated with corresponding Alexa Fluor 488 antibodies or Alexa Fluor 647 (1:200, Thermo Fisher Scientific) for 1 hour.

Slides were either developed by NBT/BCP solution (in situ hybridization, Merck) or mounted with a mounting medium with DAPI (FISH, Vectashield, 2B Scientific, Kirtlington, United Kingdom). Images were taken using THUNDER imager 3D cell culture (Leica, Wetzlar, Germany).

miRNA-148a gene target predictions

Putative miR-148a target genes were aligned from three different prediction algorithms as done previously (Ahmed et al., 2014): TargetScan (<http://www.targetscan.org/>) predicts biological targets of microRNAs by searching for the presence of conserved sites that match the seed region of each microRNA, miRanda (<http://microrna.sanger.ac.uk>) uses an algorithm to predict microRNA–mRNA pairs, and miRDB (<http://mirdb.org/>) uses miRNA–target interactions from high-throughput sequencing experiments.

Luciferase reporter assay

HaCaT cells were grown in DMEM media (Thermo Fisher Scientific) as described previously (Ahmed et al., 2014, 2011; Aunin et al., 2017; Mardaryev et al., 2010) at 37 °C with 5% carbon dioxide until 70% confluent. The 3' untranslated region fragments of *Rock1* and *Elf5* incorporating miR-148a-binding site were amplified from C57Bl/6 wild-type mouse genomic DNA using forward and reverse primers containing XhoI and NotI restriction sequences. *ELF5* sequences (5'-CTCGAGACACAGCATCGATCTCTTCTCT-3' and 5'-GCGGCCAGTTAGGGTTCAGGGCACTC-3') and *ROCK1* sequences (5'-CTCGAGTTGGGAAGTGGGAGAAGAGG-3' and 5'-GCGGCCGCGGGTAAATGCAACTTCCACTGA-3') were used. PCR products were incorporated into psiCHECK2 plasmid (Promega, Southampton, United Kingdom) using a Zero blunt cloning kit (Thermo Fisher Scientific). Mutated binding sequences were generated using a Q5 Site-directed mutagenesis kit (New England Biolabs, Hitchin, United Kingdom) as per the manufacturer's instruction. All plasmids were verified by Sanger sequencing (Source Biosciences, Nottingham, United Kingdom).

HaCaTs were cotransfected with 100 ng generated plasmid and 200 nM pro-miR-148a or miRNA control using lipofectamine 3000 into 96-well-plates. Twenty-four hours after transfection, relative luciferase activities were measured using Dual-Glo luciferase assay system (Promega) as per the manufacturer's instruction. Luminescence was measured using CLARIOStar plate reader (BMG Labtech, Ortenberg, Germany). Data from five independent experiments were pooled, \pm SEM was calculated, and statistical analysis was performed using unpaired Student's *t*-test.

Alkaline phosphatase staining

Detection of endogenous alkaline phosphatase was performed as described previously (Ahmed et al., 2014; Mardaryev et al., 2010). In brief, acetone-fixed cryosections

(10 μ m) were incubated in developing solution (100 mM sodium chloride, pH8.3, 100 mM Tris, pH 9.5, 20 mM hydrogen chloride, 0.05% Naphthol ASBI phosphate, 0.5% dimethylformamide, 25 mM sodium nitrite, and 5% New fuchsin) for 15 minutes, washed, and immersed into hematoxylin nuclear counterstain solution (Vector Laboratories, Burlingame, CA) for 45 seconds at room temperature. Images were captured using Leica THUNDER imager 3D cell culture (Leica).

Immunohistochemistry

For immunohistochemical analysis, 4% paraformaldehyde-fixed cryostat sections (10 μ m) were blocked with 0.2% Triton-X-100/PBS, 5% fetal calf serum, 2% BSA, and 10% normal goat and/or donkey serum (Merck) and incubated with primary antibodies against Rock1, Elf5, keratin 1, or keratin 15 (Supplementary Table S2) overnight at 4 °C. The following day, slides were incubated with the corresponding Alexa Fluor 488 or Alexa Fluor A555 (Supplementary Table S2) secondary antibodies for 1 hour at room temperature. Incubation steps were interspersed with wash steps with 0.2% Triton-X-100/PBS. Sections were mounted with a mounting medium with DAPI. Images were taken using Leica THUNDER imager 3D cell culture (Leica).

Immunocytochemistry

For immunocytochemical analysis, PMEKs were transfected with pro-miR-148a and miRNA control as described earlier. This was followed by treatment with high calcium (1.8 mM) for a further 48 hours after transfection. Cells were fixed with 4% paraformaldehyde and blocked with 0.2% Triton-X-100/PBS, 5% fetal calf serum, 2% BSA, and 10% normal goat and/or donkey serum. Cells were incubated with primary antibodies against Elf5 and Rock1 (Supplementary Table S2) overnight at 4 °C. Slides were then incubated with the corresponding Alexa Fluor 488 secondary antibody for 1 hour at room temperature. Incubation steps were interspersed with wash steps with 0.2% Triton-X-100/PBS. Cells were mounted with a mounting medium with DAPI. Images were taken using Leica THUNDER imager 3D cell culture (Leica).

Immunofluorescence quantification analysis

Immunofluorescence intensity analysis was determined using ImageJ software (<https://imagej.nih.gov/ij/>), as described previously (Ahmed et al., 2014). In brief, red or green fluorescent signals were collected from experimental tissues in RGB format using the same exposure conditions. To measure the fluorescence intensity at each pixel, the RGB images were converted to 16-bit grayscale format. Regions of interest (cells/epidermis and/or hair follicles) of distinct sizes within the controls, anti-miR-148a, and/or pro-miR-148a were selected, and the mean values of intensity were calculated for each selected area followed by the normalization relative to the number of DAPI⁺ cell fluorescence intensity.

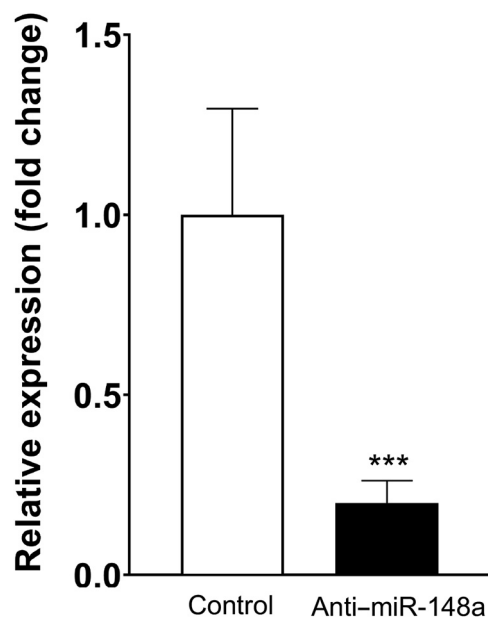
Production of lentiviruses

Human embryonic kidney 293T cells were cultured in DMEM (Thermo Fisher Scientific), supplemented with heat-inactivated 10% fetal bovine serum, 1% L-glutamine, and 5% nonessential amino acids (Thermo Fisher Scientific) at

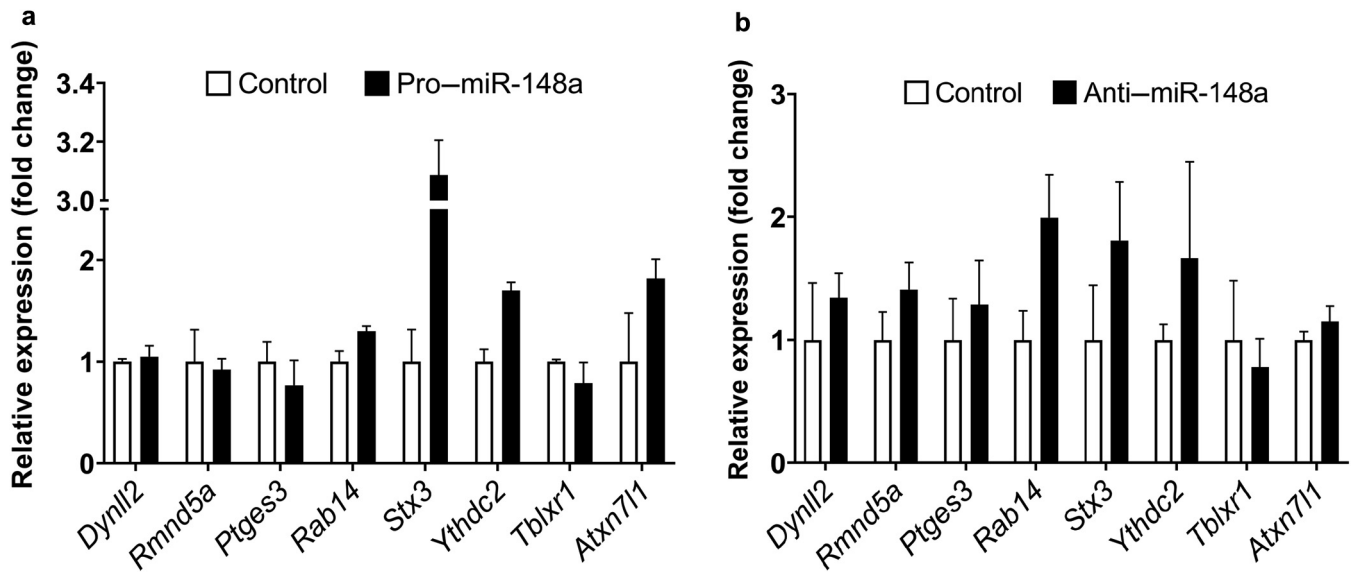
37 °C with 5% carbon dioxide. For production of MiRZIP-148a (inhibition) or short hairpin RNA control lentiviruses, at 40% confluence, human embryonic kidney 293T cells were cotransfected with MiRZIP-148a plasmid (Cambridge Biosciences) or pGFP-C-shLenti short hairpin RNA vector control (Insight Biotechnology, Wembley, United Kingdom) with packaging plasmid using Lenti-VPK packaging kit (Insight Biotechnology) following manufacturer's instructions. Cell culture medium containing viruses was collected 24 and 48 hours after transfection, followed by precipitation of the viral particles using 80 µg/ml polybrene (Thermo Fisher Scientific) and 80 µg/ml chondroitin sulfate C (Merck) for 18 hours at 4 °C before centrifugation at 10,000g. Titration of lentiviral particles was performed using qPCR lentivirus titration kit (NBS Biological, Huntingdon, United Kingdom) as per the manufacturer's instruction.

SUPPLEMENTARY REFERENCES

- Ahmed MI, Alam M, Emelianov VU, Poterlowicz K, Patel A, Sharov AA, et al. MicroRNA-214 controls skin and hair follicle development by modulating the activity of the Wnt pathway. *J Cell Biol* 2014;207:549–67.
- Ahmed MI, Mardaryev AN, Lewis CJ, Sharov AA, Botchkareva NV. MicroRNA-21 is an important downstream component of BMP signalling in epidermal keratinocytes. *J Cell Sci* 2011;124:3399–404.
- Ahmed MI, Pickup ME, Rimmer AG, Alam M, Mardaryev AN, Poterlowicz K, et al. Interplay of MicroRNA-21 and SATB1 in epidermal keratinocytes during skin aging. *J Invest Dermatol* 2019;139:2538–42.e2.
- Aunin E, Broadley D, Ahmed MI, Mardaryev AN, Botchkareva NV. Exploring a Role for Regulatory miRNAs In Wound Healing during Ageing: involvement of miR-200c in wound repair. *Sci Rep* 2017;7:3257.
- Mardaryev AN, Ahmed MI, Vlahov NV, Fessing MY, Gill JH, Sharov AA, et al. Micro-RNA-31 controls hair cycle-associated changes in gene expression programs of the skin and hair follicle. *FASEB J* 2010;24:3869–81.
- Pickup ME, Ahmed MI. Detection of microRNAs by in situ hybridization in skin. In: Botchkareva NV, Westgate GE, editors. *molecular dermatology: methods and protocols*. New York: Springer; 2020. p. 187–96.

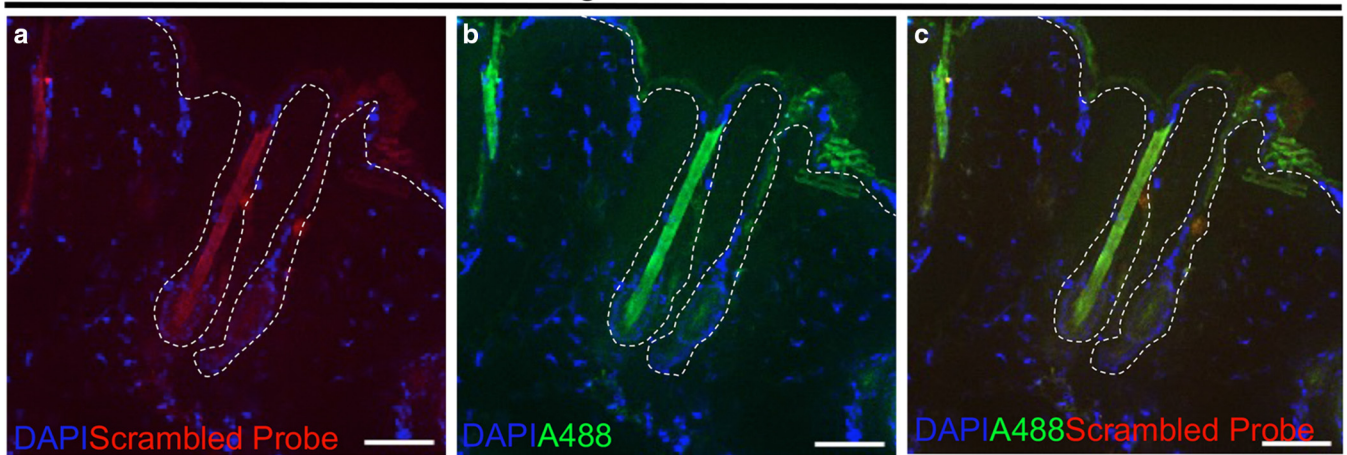


Supplementary Figure S1. Confirmation of miRNA-148a inhibition in vivo. (a) Inhibition of miR-148a was confirmed by TaqMan RT-qPCR analysis of pharmacologically inhibited miR-148a skin samples, which revealed a significant reduction in miR-148a expression in anti-miR-148a-treated skins compared with that of the control skins. $n = 3$ mice per treatment. Data are presented as mean \pm SEM (error bars). *** $P < 0.001$ by Student's t -test.

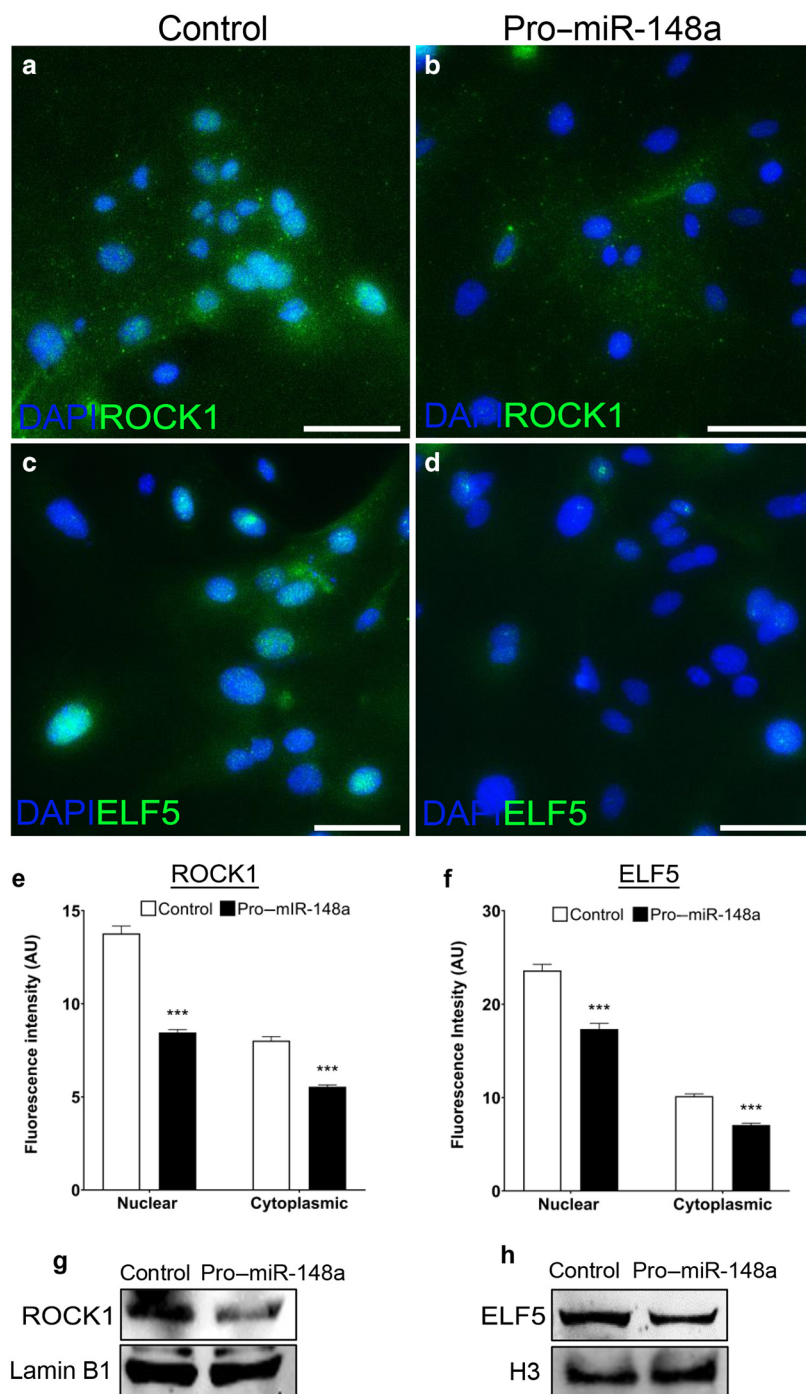


Supplementary Figure S2. RNA sequencing data validation. (a, b) RT-qPCR analysis of predicted target genes that were highly conserved between human and mouse genomes from our RNA-sequencing data and which had predictive binding sites from miRNA target databases (from Figure 3). No significant effects were observed after the modulation of miR-148a activity in primary mouse epidermal keratinocytes. Data are presented as mean \pm SEM values from three independent experiments. miRNA, microRNA.

Negative controls



Supplementary Figure S3. Controls of miRNA-148a FISH with immunofluorescent staining. (a–c) The negative controls using scrambled probe (red) and Alexa fluor 488 (A488, green) counterstained with DAPI (blue) detections for Figure 3h and i. No specific staining was observed for negative controls. Images are representative microphotographs of staining. The broken lines demarcate the epidermal–dermal border. Bars = 50 μ m.



Supplementary Figure S4. miRNA-148a inhibits nuclear localization of ROCK1 and ELF5 in keratinocytes. (a-d)

Immunocytochemistry staining of ROCK1 and ELF5 during calcium-induced (1.8 mM) keratinocyte differentiation after overexpression of miR-148a in PMEKs. A reduction of ROCK1 and ELF5 expression in the nucleus as well as cytosol was observed after pro-miR-148a (overexpression) treatment versus control cells. (e, f) Quantitative immunofluorescence intensity analysis after pro-miR-148a versus control treatments in PMEKs. A significant inhibitory effect of miR-148a on ROCK1 (green) and ELF5 (green) expression is observed in the nucleus and cytosol compared with those in the control cells normalized to DAPI⁺ cells. Data are presented as mean \pm SEM values from 100 cells counted per treatment from three independent experiments. (g, h) Nuclear localization of ROCK1 and ELF5 was analyzed by western blot during calcium-induced keratinocyte differentiation in PMEKs: overexpression of miR-148a reduced (g) ROCK1 and (h) ELF5 nuclear protein levels compared with that of the controls. Data shown are from a single representative experiment of three experimental repeats. Fraction purity of western blots was confirmed using antibodies against nuclear Histone H3 and Lamin B1 marker proteins. *** $P < 0.001$ by Student's *t*-test. Bars = 50 μ m. PMEK, primary mouse epidermal keratinocyte.